Turbulent bursting and spatiotemporal intermittency in the counterrotating Taylor-Couette system

Peter W. Colovas* and C. David Andereck
Department of Physics, The Ohio State University, 174 West 18th Avenue, Columbus, Ohio 43210
(Received 15 July 1996)

Turbulent bursting that is intermittent in time and space occurs in the Taylor-Couette system when the cylinders rotate in opposite directions. We show, through an analysis of the turbulent fraction and the size distributions of turbulent and laminar domains, that the Taylor-Couette system behaves differently than previously explored systems exhibiting spatiotemporal intermittency. Finally, we consider the analogy linking spatiotemporal intermittency with second order phase transitions. [S1063-651X(97)00803-9]

PACS number(s): 47.27.Cn, 47.20.Ky, 47.52.+j

I. INTRODUCTION

Spatiotemporal intermittency (STI) is a state of extended pattern forming systems in which turbulent and laminar patches coexist at a fixed value of the control parameter. This behavior has been observed in a variety of systems. Theoretical studies include systems of partial differential equations (PDE's), such as the damped Kuramoto-Sivashinsky equation [1], coupled map lattices [2–5], and cellular automata [6]. Experimentally, STI has been observed in Rayleigh-Bénard convection, in both narrow channels [7] and annuli [8]. It has also been observed in the horizontal partially filled gap between eccentric cylinders (the printer's instability) [9], in the wetting of the internal surface of a single rotating horizontal cylinder, in the Faraday experiment [10–12], and most recently in the Taylor-Dean system [13]. These systems are all essentially one-dimensional extended systems (except for the Faraday experiment), which exhibit complex spatiotemporal dynamics. Recent studies of STI have concentrated on exploring the conjecture of Pomeau [14], which suggests an analogy between STI and a second order phase transition in thermodynamic systems, similar to that occurring in directed percolation.

The nature of the STI transition is that above a critical value of the control parameter there appear in the system turbulent patches in a ''laminar'' background (what is meant by ''laminar'' will be described below). In the usual analogy, these turbulent patches are assumed equivalent to the ''active'' or ''contaminating'' state in directed percolation, while the laminar background is the ''passive'' or ''absorbing'' state. The population statistics of these states have been used to characterize the transition to turbulence via spatiotemporal intermittency and to show that the behavior approximates a second order phase transition. Previous experiments have shown that the numbers resulting from such a statistical analysis differ across the systems showing STI, so that the transition may not exhibit universality. In this paper we examine states of flow between concentric cylinders which rotate in opposite directions, and show that they exhibit the essential characteristics of STI.

Turbulent bursts occurring in Taylor-Couette flow, the flow between two concentric rotating cylinders, were observed by Coles [15] and were further characterized by Andereck, Liu, and Swinney [16], who catalogued the various patterns in the Taylor-Couette system. A photograph of the bursts is shown in Fig. 1. Until recently, however, this flow regime had been noted merely as an interesting precursor to spiral turbulence, the barberpole pattern of intertwined helical turbulent and laminar regions described by Feynman in his lectures [17]. Numerical work by Coughlin and Marcus [18] may provide a mechanism for the bursting behavior observed here, as well as other bursting phenomena observed by Hamill *et al.* [19], in Taylor-Couette systems with lower radius ratios.

II. EXPERIMENTAL APPARATUS AND PROCEDURES

The experimental system is a concentric Taylor-Couette apparatus with the two cylinders driven independently. The radius of the outer cylinder $r_o = 5.96$ cm, while that of the inner cylinder $r_i = 5.26$ cm. The width of the gap is $d = r_o - r_i = 0.70$ cm, the radius ratio $\eta = r_i / r_o = 0.882$, and the aspect ratio $\Gamma = l/d = 70$, where l is the axial length of the system. The conditions at both ends of the apparatus are fixed, with the end rings attached to the outer cylinder. We used three fluids in the system over various runs, water,

FIG. 1. Photograph of turbulent bursts in laminar background, for $R_o = -1650$, $R_i = 556$.

*Present address: Anderson Consulting LLP, 3773 Willow Road, Northbrook, IL 60062.

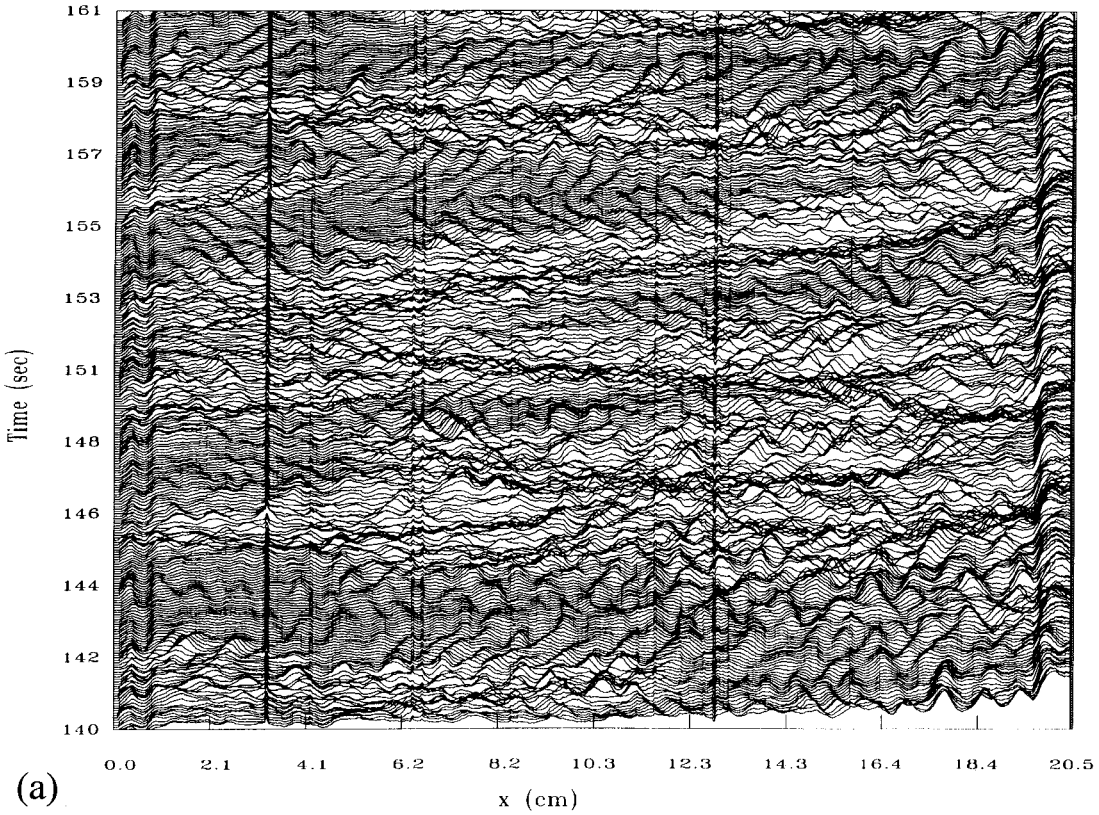

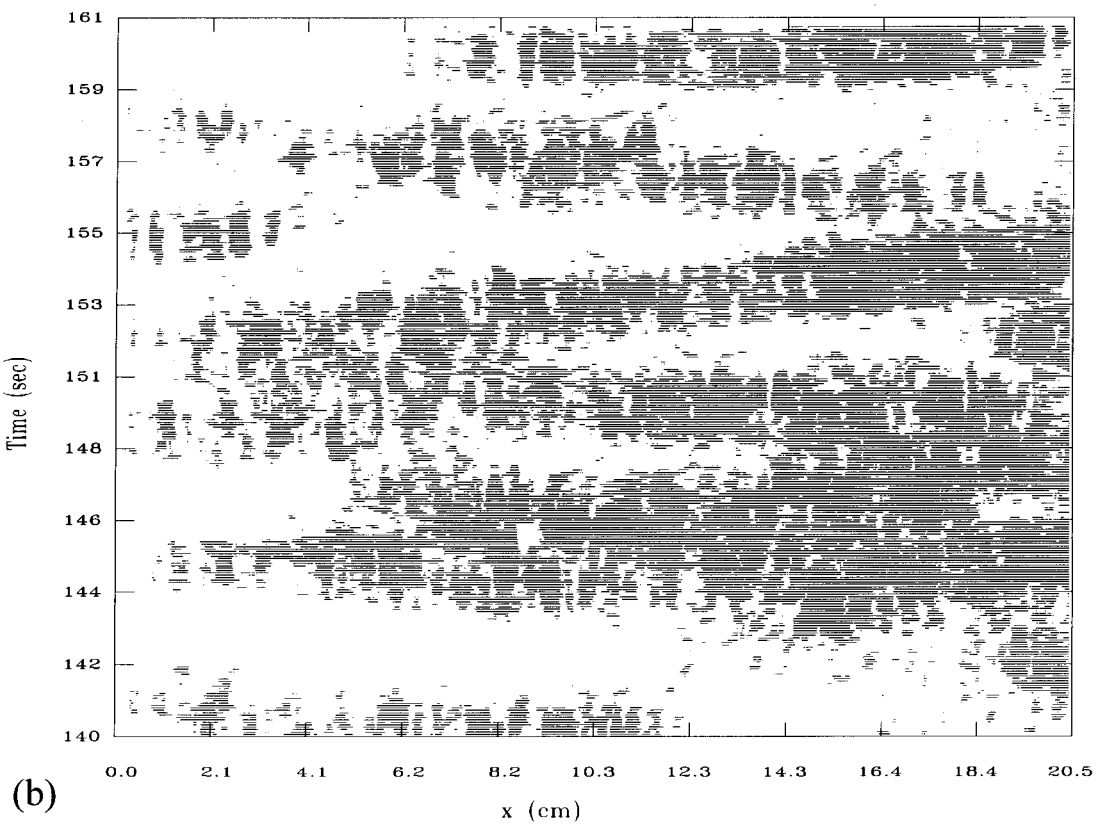

FIG. 2. Reduction of space-time data for the state pictured in Fig. 1. (a) Raw data as recorded by 1024 pixel CCD camera, (b) binarized plot showing turbulent (dark) and laminar (white) domains.

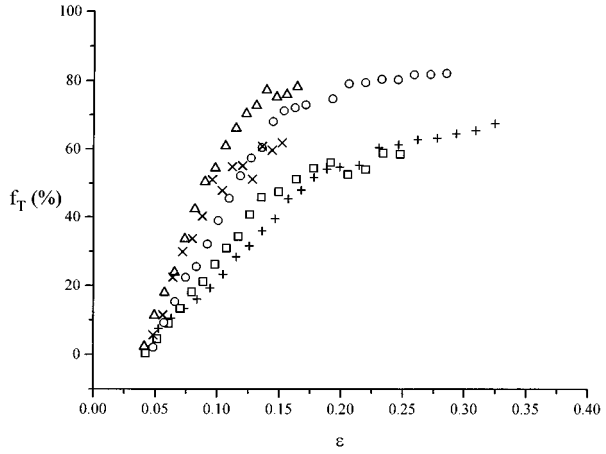

FIG. 3. Turbulent fraction f_T plotted against ϵ for $R_o=-1150(+)$, $-1450(\square)$, $-1650(\bigcirc)$, $-1850(\Delta)$, and $-1950(\times)$. $\epsilon_T=0.052$ for all R_o, and the increase of f_T is initially linear with ϵ.

which has kinematic viscosity $\nu=0.98\times10^{-2}$ cm^2/sec, and two glycerol-water mixtures, 28% glycerol by weight, and 45% glycerol by weight, which have $\nu=2.14\times10^{-2}$ and 3.14×10^{-2} cm^2/sec, respectively. Visualization of the pattern in all three fluid mixtures was accomplished by the addition of 1% by volume of Kalliroscope AQ 1000 polymeric flakes. The inner and outer cylinders are independently driven by Compumotor stepper motors, giving two control parameters $R_o=\Omega_o r_o d/\nu$ and $R_i=\Omega_i r_i d/\nu$, which nondimensionalize the outer and inner cylinder speeds, respectively.

The (R_o,ϵ) plane is investigated in the following manner: The outer cylinder speed is fixed at the desired R_o, and then the inner cylinder speed is increased quasistatically, so that the system will pass slowly through each flow state of interest. For each ϵ where data are to be taken, the system is left for 15 min to allow transients to die out. After equilibration, data are taken with a 1024 pixel linear array charge coupled device (CCD) camera, which records the intensity profile of the light reflected by the Kalliroscope flakes, and images a vertical (axial) line along the middle 21 cm of the system. A

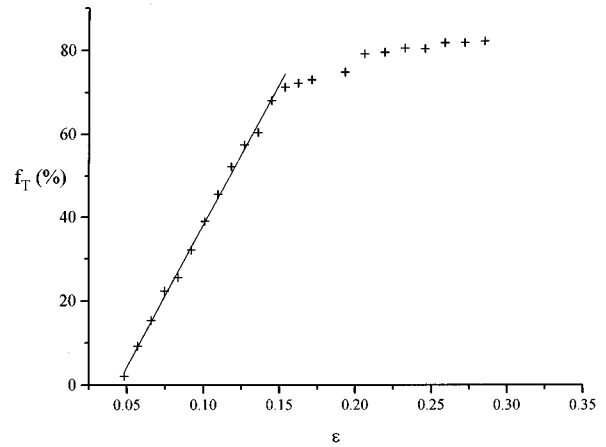

FIG. 4. Turbulent fraction f_T as a function of ϵ for $R_o=-1650$. The line is given by $f_T\sim640.5\ \epsilon$.

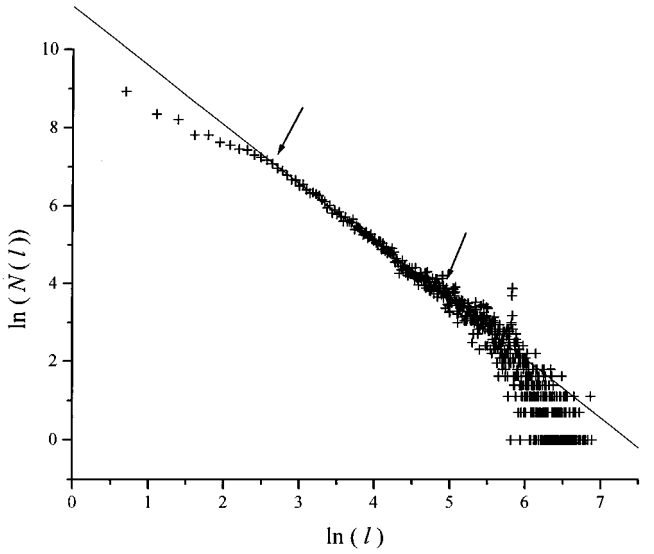

FIG. 5. Histogram showing the distribution $N(l)$ of laminar domains of length l. This example is for $R_o=-1450$ and $\epsilon=0.079$. The fit is between the points marked with arrows, and covers a range in l of two decades.

frame is taken every 0.14 sec for pure water in the system, and every 0.07 sec for the glycerol-water mixtures. A typical data file consists of 5000 frames, which is approximately 12 min of data for the water system, and 6 min for the glycerol-water system. A representative space-time plot of the raw data is shown in Fig. 2(a).

To do the statistical analysis, it is first necessary to distinguish between the laminar and turbulent domains in a consistent manner. While other groups have used simple amplitude- [8] or wavelength- [7] based cutoffs to differentiate between types of domains, we have chosen another method, one that takes advantage of the abruptly different character of the laminar and turbulent states of flow. To this end, we have used a frequency-based differentiation scheme to distinguish turbulence from laminar flow.

The procedure is to slide a 16 point window along the

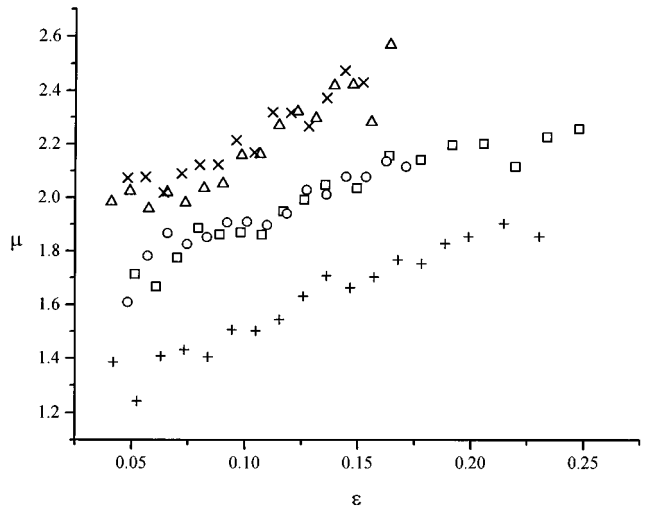

FIG. 6. Variation of laminar decay power μ with ϵ. The R_o values are as in Fig. 3.

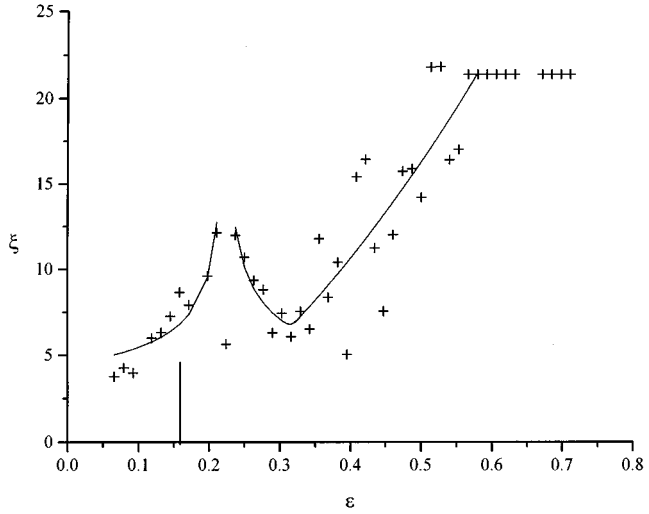

FIG. 7. Correlation length as calculated from the binary data representation for $R_o=-1650$. The lines indicate the divergence of the correlation length and the increase in coherence due to spiral turbulence. The vertical line marks the approximate onset of spiral turbulence.

time direction, checking the spectrum at each point against three Fourier frequencies; if all three are above an arbitrary cutoff, then the first point is marked turbulent. The three frequencies used to discriminate are chosen by comparing 16 point power spectra from laminar domains against those from turbulent domains and using the three peaks which are most prominent in the turbulent domain. The results of the data reduction are shown in Fig. 2(b), where the turbulent regions are dark, and the laminar regions are white. The results of this procedure are verified by eye, to be certain that all significant features have been accounted for.

III. OBSERVATIONS AND ANALYSIS

The base flow in the counter-rotating Taylor-Couette system is a featureless state known as Couette flow, a two-dimensional purely azimuthal flow caused by the cylinders pulling the fluid around the annulus. The flow is divided by a nodal surface at r_n, which is defined by $v_\phi(r=r_n,\phi,z,t)=0$. Flow within this surface ($r<r_n$) is linearly and centrifugally unstable to the formation of interpenetrating spiral vortices (IPS) above a certain value $R_i=R_{ic}$, which differs for different values of $\mu=R_o/R_i$. Outside the nodal surface the flow is stable. We express our results in terms of a reduced inner cylinder Reynolds number $\epsilon=(R_i-R_{ic})/R_{ic}$, so that $\epsilon=0$ at the transition to the first time-dependent state. For a Couette system with our value for η, there is a range of R_o, $-1000\lesssim R_o\lesssim -2000$, where the interpenetrating spirals become unstable to a state in which turbulent spots appear in the spiral background, for $\epsilon>\epsilon_T$. As ϵ is increased, the background spirals become more faint, until the spots appear to coexist with a featureless background. As ϵ increases further, the spots begin to arrange themselves into a spiral structure, until at the point $\epsilon=\epsilon_{\mathrm{ST}}$ the turbulence becomes arranged into spiral turbulence, which has been well described elsewhere [15,16,20,21]. The state of turbulent bursting bears a remarkable resemblance to the spatiotemporally intermittent states described above, and its further statistical analysis is the main subject of this paper.

Closer observation of the system in the turbulent bursting regime reveals two distinct processes occurring. In the first, appearing just above the onset of STI, ϵ_{STI}, turbulent spots are generated spontaneously from perturbations in the IPS state, as described by Coles [15]. These spots are of finite size and have a finite lifetime, and there may be periods of time during which no turbulence is seen in the system. At higher values of ϵ turbulent domains are always present in the system, and they spread and move around the system in a way that is reminiscent of directed percolation [14], although there is some question as to whether STI falls into the same universality class [22,23].

Using the binary representation of the data, we first calculate a time averaged spatial turbulent fraction (simply referred to as the turbulent fraction f_T), which serves as the order parameter in the phase transition analogy. f_T is plotted across the range of R_o where STI occurs in Fig. 3. The plot of f_T shows that bursting in the system begins near $\epsilon_T=0.04$, independent of R_o. The turbulent fraction rises linearly with increasing ϵ for each value of R_o until crossing into spiral turbulence, indicated in Fig. 3 by a flattening of the turbulent fraction curves. The linear nature of the increase is shown for $R_o=-1650$ in Fig. 4. The value of ϵ_{ST} is roughly given by $\epsilon_{\mathrm{ST}}\simeq 0.41-0.000\,16|R_o|$. The increasing slope of f_T with increasing R_o is consistent with the narrowing of the range of ϵ where bursts occur, as illustrated in Ref. [16].

Following the analysis of Chaté and Manneville [1], we have also calculated from the binary data representation the distribution of laminar lengths $N(l)$ of length l (Fig. 5). Starting just above the transition point ϵ_T, this distribution is characterized by an algebraic decay, $N(l)\sim l^{-\mu}$, for all values of R_o and ϵ where turbulent bursts are observed. The magnitude of μ increases with increasing ϵ and increasing $|R_o|$, as shown in Fig. 6, with dependence

TABLE I. Summary of exponents characterizing STI in various experimental systems.

Experimental system	β	μ_s	α_s	ν	ν'
Convection in annulus [8]		1.9 ± 0.1	0.5		
Convection in channel [25]	0.3 ± 0.05	1.6 ± 0.2	0.50 ± 0.05		
Convection in annulus [25]		1.7 ± 0.1	~0.50		
Roll coating system [9]	0.45 ± 0.05	0.63 ± 0.02	0.50		
Taylor-Dean system [13]	1.33 ± 0.26	1.67 ± 0.14	$\simeq0.64$	$\simeq0.53$	$\simeq1.20$
Taylor-Couette system	1	$1.4-2.5$		$\simeq0.3$	$\simeq0.4$

$\mu \sim 0.000\,73|R_o| + 3.45(\epsilon - \epsilon_T)$.

A second order phase transition is characterized by an increase in the order parameter of the form $f_T \sim (\epsilon - \epsilon_c)^{1/2}$, while the order parameter for these states in the Taylor-Couette system increases linearly. Additionally, the statistical analysis done by Chaté and Manneville [1] shows a crossover in the behavior of the distribution $N(l)$ at the critical point ϵ_c, from algebraic decay to exponential decay, i.e., $N(l) \sim e^{-l/m}$. The lack of a region of exponential decay of $N(l)$, coupled with the linear growth of f_T, would seem to indicate that the turbulent bursting present in the Taylor-Couette system is not evidence of a transition via spatiotemporal intermittency. However, Grassberger and Schreiber [23] have shown that the nature of the transition may be changed by the emergence of other coherent structures in the system. In this case, the barberpole structure of spiral turbulence may be involved.

An explanation of the finite width of the spirals in spiral turbulence has been given by Hegseth *et al.* [20] and Hayot and Pomeau [24]. They describe the behavior as an effect of the pressure induced backflow due to the azimuthal and axial confinement of the system. It is believed that the same mechanism is responsible for limiting the size of the spots in the bursting state [25].

To explore the existence of a hidden phase transition we examined the behavior of the spatial correlation length as calculated from the binary data representation. The correlation function is of the form

$$C_b(x) = \frac{\langle [\tilde{I}(z+x,t)][\tilde{I}(z,t)] \rangle}{\langle \tilde{I}(z,t)^2 \rangle},$$

where $\tilde{I}$ is zero for a laminar point, and 1 for a turbulent point. Figure 7 shows the correlation length for $R_o = -1650$. Although the scatter in the data increases significantly above $\epsilon \simeq 0.3$, behavior suggesting a divergence of the correlation length is visible, centered at $\epsilon = 0.22$, which is near the onset point for spiral turbulence. The ϵ dependence of the correlation length is given by $\xi \sim (\epsilon_c - \epsilon)^{\nu'}$ for $\epsilon < \epsilon_c$, and $\xi \sim (\epsilon - \epsilon_c)^{-\nu}$ for $\epsilon > \epsilon_c$. In our system, $\nu' \simeq 0.3$ and $\nu \simeq 0.4$. This is evidence that a phase transition may be present in the system, but is modified by the appearance of the large scale organization of spiral turbulence in the system. Figure 7 also shows a steady increase in the correlation length above $\epsilon = 0.3$, which coincides with the emergence of spiral turbulence in the system.

Similar analysis of the lifetimes of the spots shows no divergence of either the lifetimes of the turbulent spots or the laminar spots in the system.

IV. CONCLUSIONS

Our study of turbulent bursting phenomena in a Taylor-Couette apparatus of radius ratio $\eta = 0.88$ has revealed behavior that resembles the spatiotemporal intermittency observed in other quasi-one-dimensional systems, namely, the distribution of laminar domains $N(l)$ just above ϵ_T, and the existence of an order parameter f_T which shows an abrupt transition at $\epsilon_T = 0.052$. A divergence of the correlation length may also be present, and provides some evidence that the transition is disturbed by the large scale coherence of spiral turbulence. A similar divergence of the correlation length has also been reported by Degen *et al.* [13]. We list the exponents characterizing various intermittent systems in Table I, and note that all of these systems exhibit characteristics of STI, although the exponents differ from system to system. This seems to support the argument [23,13] that the properties of the ''laminar'' state play a nontrivial role in the manifestation of STI.

While our study has concentrated on the statistical aspects of the turbulent burst state, other recent work [18] has described a possible mechanism for the generation of the turbulent bursts themselves. These may be produced by an azimuthally traveling modulation near the nodal surface $r = r_n$ which extends into the region $r > r_n$ as the amplitude of the spiral instability grows larger. This triggers a burst through a shear instability, which then draws energy from the laminar outer region. When the burst depletes the energy of the outer region, it collapses, and the process begins again. This instability may be responsible for creating a ''pre-STI'' region, which has also been observed in studies of spatiotemporal intermittency in Rayleigh-Bénard flow in an annulus [26]. This ''pre-STI'' region results in a turbulent fraction which also appears to grow linearly.

ACKNOWLEDGMENTS

We would like to acknowledge I. Mutabazi, P. Marcus, M. Degen, and Y. Pomeau for their thoughts and discussion.

[1] H. Chaté and P. Manneville, Phys. Rev. Lett. **58**, 112 (1987).
[2] H. Chaté and P. Manneville, Physica (Amsterdam) D **32**, 409 (1988).
[3] K. Kaneko, Prog. Theor. Phys. **58**, 112 (1987).
[4] K. Kaneko, Physica (Amsterdam) D **34**, 1 (1989).
[5] J. R. de Bruyn and L. Pan, Phys. Rev. E **47**, 4575 (1993).
[6] H. Chaté and P. Manneville, J. Stat. Phys. **56**, 357 (1989).
[7] F. Daviaud, M. Dubois, and P. Bergé, Europhys. Lett. **9**, 441 (1989).
[8] S. Ciliberto and P. Bigazzi, Phys. Rev. Lett. **60**, 286 (1988).
[9] S. Michalland, M. Rabaud, and Y. Couder, Europhys. Lett. **22**, 17 (1993).
[10] N. B. Tufillaro, R. Ramshankar, and J. P. Gollub, Phys. Rev. Lett. **62**, 422 (1989).
[11] B. J. Gluckman, P. Marcq, and J. P. Gollub, Phys. Rev. Lett. **71**, 2034 (1993).
[12] E. Bosch and W. van de Water, Phys. Rev. Lett. **70**, 3420 (1993).
[13] M. M. Degen, I. Mutabazi, and C. D. Andereck, Phys. Rev. E **53**, 3495 (1996).
[14] Y. Pomeau, Physica (Amsterdam) D **23**, 3 (1986).
[15] D. Coles, J. Fluid Mech. **21**, 385 (1965).
[16] C. D. Andereck, S. S. Liu, and H. L. Swinney, J. Fluid Mech. **164**, 155 (1986).

[17] R. P. Feynman, *Lectures on Physics* (Addison-Wesley, Reading, MA, 1964), Vol. 2.
[18] K. Coughlin and P. S. Marcus, Phys. Rev. Lett. **77**, 2214 (1996).
[19] F. Hamill, A. Predtechensky, E. Sha, and H. L. Swinney (unpublished).
[20] J. J. Hegseth, C. D. Andereck, F. Hayot, and Y. Pomeau, Phys. Rev. Lett. **62**, 257 (1989).
[21] C. W. van Atta, J. Fluid Mech. **25**, 495 (1966).
[22] H. Chaté and P. Manneville, in *New Trends in Nonlinear Dynamics and Pattern Forming Phenomena*, edited by P. Coullet and P. Huerre (Plenum, New York, 1990), pp. 199–214.
[23] P. Grassberger and T. Schreiber, Physica (Amsterdam) D **50**, 177 (1991).
[24] F. Hayot and Y. Pomeau, Phys. Rev. E **50**, 2019 (1994).
[25] Y. Pomeau (private communication).
[26] F. Daviaud, M. Bonetti, and M. Dubois, Phys. Rev. A **42**, 3388 (1990).